

Three-dimensional models of deformation near strike-slip faults

Uri S. ten Brink

U.S. Geological Survey, Woods Hole, Massachusetts

Rafael Katzman¹

Department of Earth, Atmospheric, and Planetary Sciences, Massachusetts Institute of Technology, Cambridge

Jian Lin

Department of Geology and Geophysics, Woods Hole Oceanographic Institution, Woods Hole, Massachusetts

Abstract. We use three-dimensional elastic models to help guide the kinematic interpretation of crustal deformation associated with strike-slip faults. Deformation of the brittle upper crust in the vicinity of strike-slip fault systems is modeled with the assumption that upper crustal deformation is driven by the relative plate motion in the upper mantle. The driving motion is represented by displacement that is specified on the bottom of a 15-km-thick elastic upper crust everywhere except in a zone of finite width in the vicinity of the faults, which we term the “shear zone.” Stress-free basal boundary conditions are specified within the shear zone. The basal driving displacement is either pure strike slip or strike slip with a small oblique component, and the geometry of the fault system includes a single fault, several parallel faults, and overlapping en echelon faults. We examine the variations in deformation due to changes in the width of the shear zone and due to changes in the shear strength of the faults. In models with weak faults the width of the shear zone has a considerable effect on the surficial extent and amplitude of the vertical and horizontal deformation and on the amount of rotation around horizontal and vertical axes. Strong fault models have more localized deformation at the tip of the faults, and the deformation is partly distributed outside the fault zone. The dimensions of large basins along strike-slip faults, such as the Rukwa and Dead Sea basins, and the absence of uplift around pull-apart basins fit models with weak faults better than models with strong faults. Our models also suggest that the length-to-width ratio of pull-apart basins depends on the width of the shear zone and the shear strength of the faults and is not constant as previously suggested. We show that pure strike-slip motion can produce tectonic features, such as elongate half grabens along a single fault, rotated blocks at the ends of parallel faults, or extension perpendicular to overlapping en echelon faults, which can be misinterpreted to indicate a regional component of extension. Zones of subsidence or uplift can become wider than expected for transform plate boundaries when a minor component of oblique motion is added to a system of parallel strike-slip faults.

Introduction

Crustal deformation associated with strike-slip (wrench) faults can be complex [e.g., *Christie-Blick and Biddle*, 1985], leading to ambiguous and even contradictory kinematic interpretations of the relative motions between blocks or plates. Analytical, numerical, and physical models have been introduced to help guide the interpretation of the observed deformation in these environments [cf. *Sylvester*, 1988]. Clay and sandbox models and recently finite element simulations were used to follow the initiation and development of faulting [e.g., *Wilcox et al.*, 1973; *Naylor et al.*, 1986; *Withjack and Jamison*, 1986; *Richard and Cobbold*, 1990; *Braun*, 1994]. Another approach, which is followed in this paper, predetermines the

location and number of fault planes on which motion occurs and studies the resulting strain and stress fields in the vicinity of these fault planes [*Segall and Pollard*, 1980; *Bilham and King*, 1989; *Gomberg and Ellis*, 1994]. Many of the previous models were two-dimensional (2-D) or three-dimensional (3-D) half-space, but *Katzman et al.* [1995] showed that 2-D approximations can lead to erroneous predictions in the vicinity of the fault tip. In this paper we treat the problem in a fully 3-D model. Some of the previous models [*Bilham and King*, 1989; *Stein et al.*, 1992; *King et al.*, 1994] examined the deformation or the stress field due to a prescribed displacement discontinuity on the fault because short-term distribution of fault movements can be measured geodetically. Our approach here is to prescribe basal displacement boundary conditions (which, we assume, represent the regional displacement) and allow the fault displacement to adjust itself depending upon the geometry and shear strength of the fault system and the width of basal decoupling. Our focus in this paper is similar to that of *Bilham and King* [1989], namely, understanding the deformation associated with strike-slip faults. Our earlier paper [*Katz-*

¹Also at MIT/WHOI Joint Program in Oceanography, Woods Hole, Massachusetts.

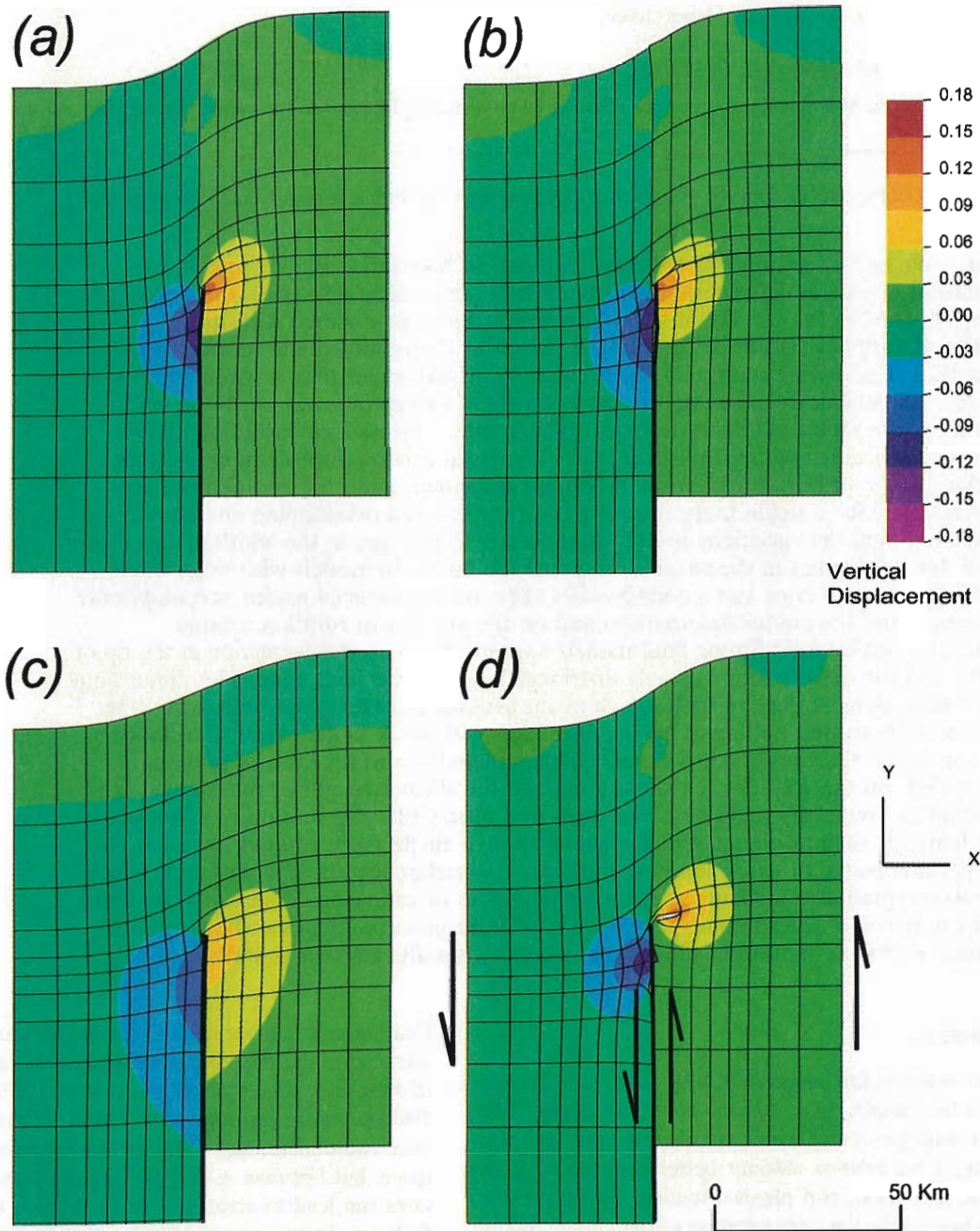


Plate 1. Effect of the shear zone: Surface deformation for models with a single, semi-infinite weak fault due to relative left-lateral basal displacement of 5 km with shear zone width of (a) zero wide; that is, basal displacement is defined adjacent to the fault trace, (b) 10 km; that is, free-stress boundary conditions exist to a distance of 5 km on either side of the fault trace, and (c) 40 km. (d) Vertical deformation due to left-lateral displacement of 5 km, which is defined directly on the fault indicated by heavy lines. Colors represent vertical displacement, and the grid represents horizontal deformation from originally rectangular mesh. Vertical deformation is normalized to the amount of imposed left-lateral displacement. Grid deformation is multiplied by a factor of 4 to enhance the pattern near the fault tips.

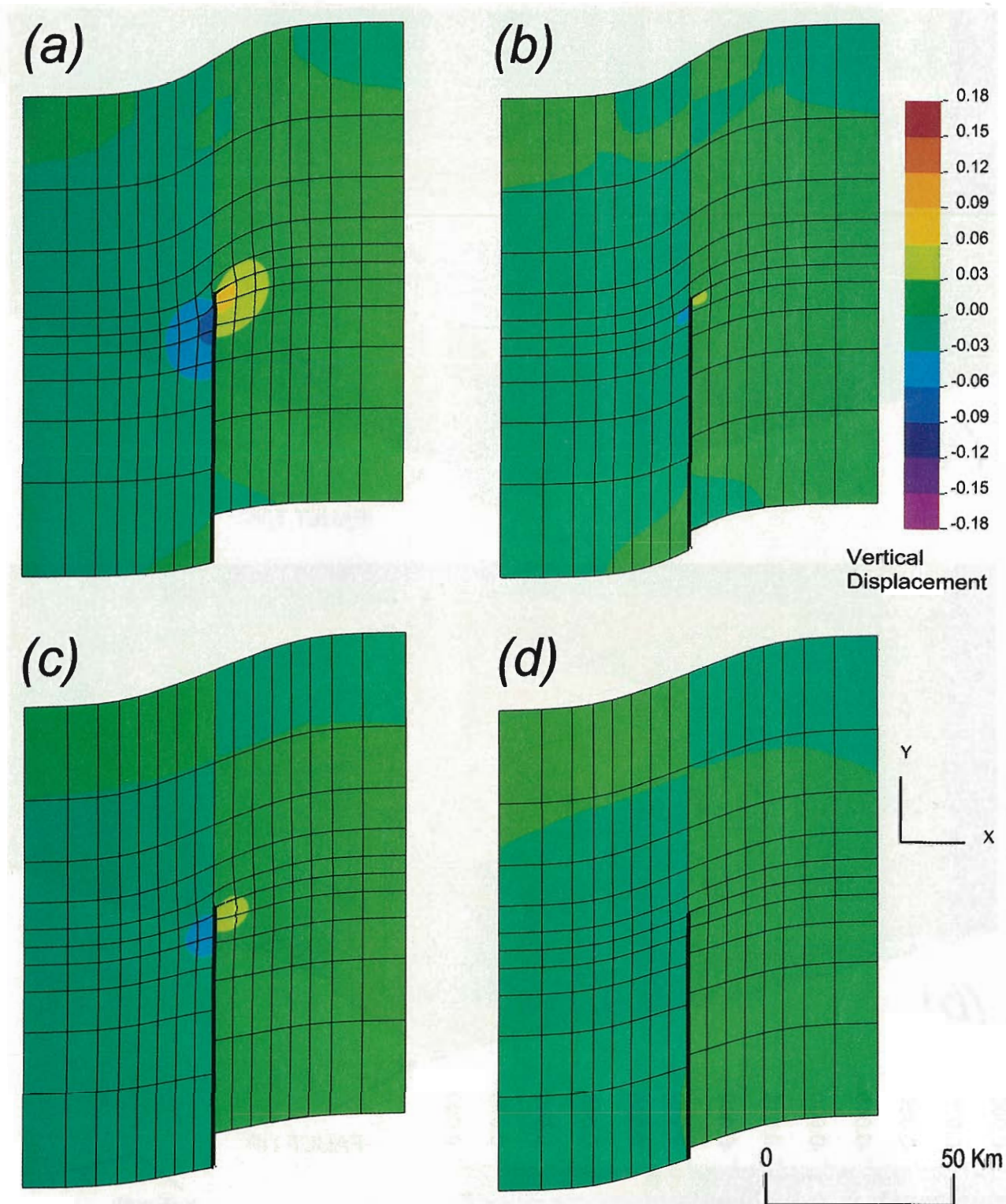
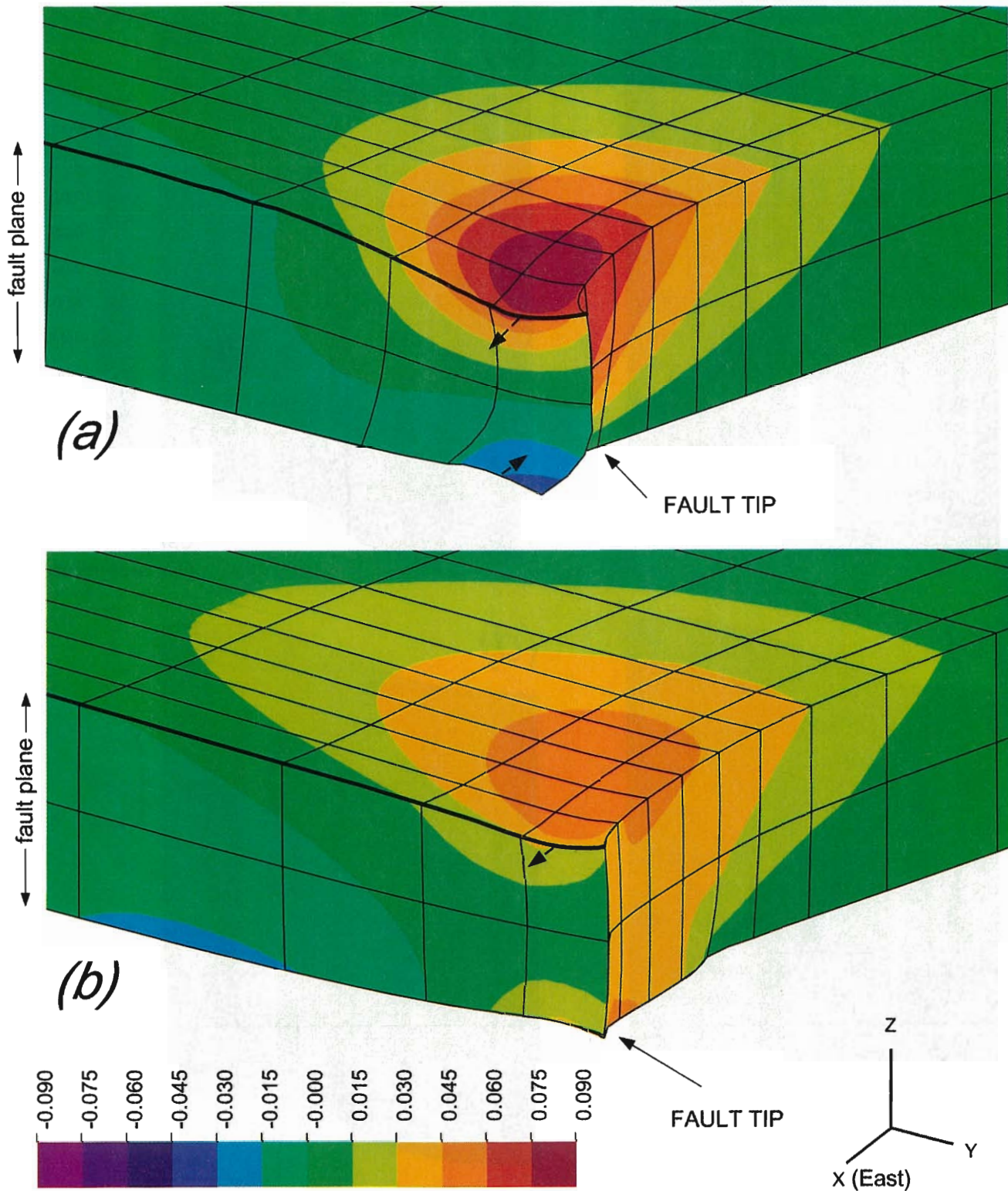


Plate 2. Effect of fault strength: Surface deformation for models with a single, semi-infinite strong fault due to relative left-lateral basal displacement of 5 km. Shear zone width is (a, b) 10 km and (c, d) 40 km. The fault's shear strength is characterized by internal springs (see text for description) and is normalized to the shear modulus of the elastic medium. Fault strength is 2% for Plates 2a and 2c and 10% for Plates 2b and 2d of the shear modulus. Colors represent vertical displacement, and the grid represents horizontal deformation from originally rectangular mesh. Vertical deformation is normalized to the amount of imposed left-lateral displacement. Grid deformation is multiplied by a factor of 4 to enhance the pattern near the fault tips.



Horizontal Displacement Perpendicular to Fault Plane

Plate 3. Isometric view of the lower left (SW) quarter of the models in Plates 1a and 1c. Colors represent horizontal displacement perpendicular to the fault plane with positive values indicated by yellow and red in the x (east or out-of-page) direction. The grid represents deformation from originally rectangular mesh. (a) A model with zero-width shear zone. (b) A model with a 40-km-wide shear zone. Arrows indicate rotation of the fault plane, and heavy lines indicate surface trace of the fault. Horizontal displacement is normalized to the amount of imposed left-lateral displacement. Grid deformation is multiplied by a factor of 4.

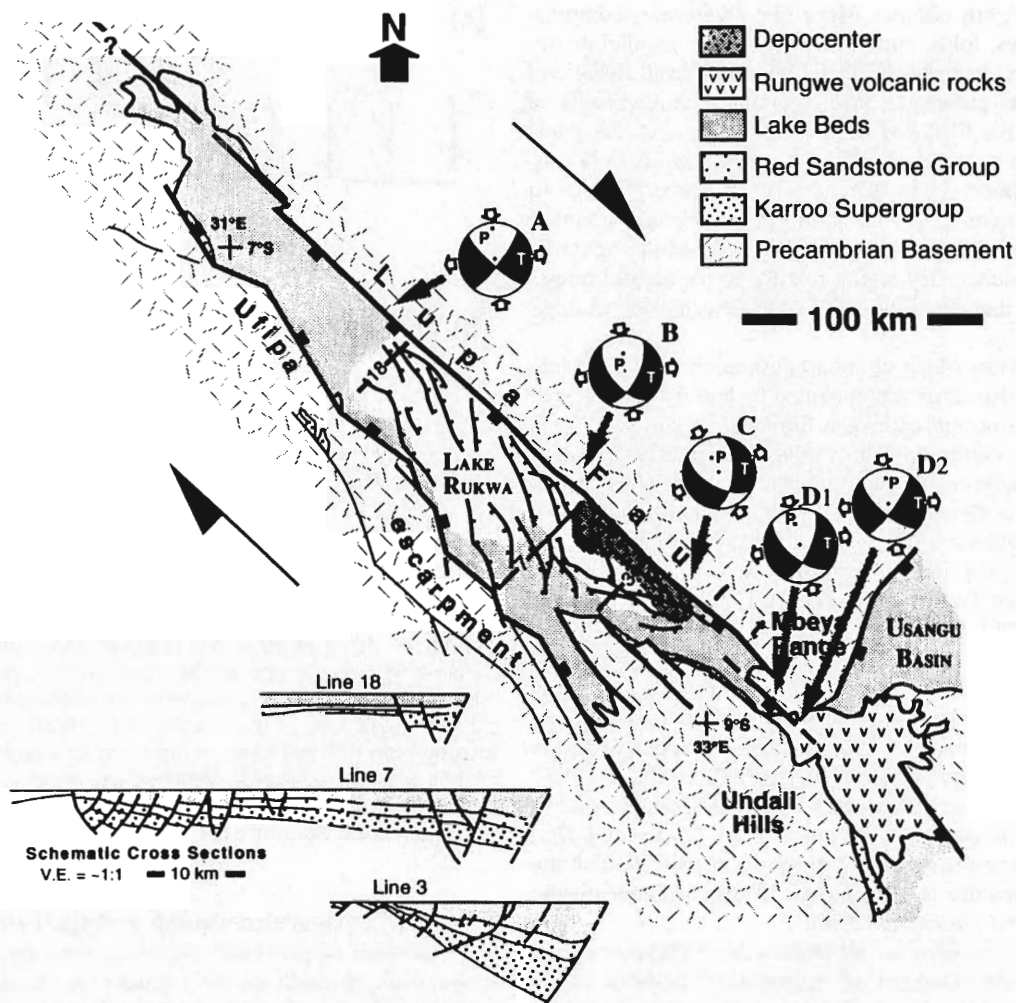


Figure 1. Simplified geology and earthquake focal mechanisms in the Rukwa rift region in the western branch of the East African rift [from *Wheeler and Karson, 1994*]. Slickensides and fault plane solutions indicate dextral strike slip on the fault and greatest subsidence component adjacent to the depocenter, which is at the SE part of the lake. Uplift is located at the Mbeya Range SE of the fault tip. Basin is a half graben with lake beds dipping NE toward the fault and SE. Barbed heavy lines indicate faults. Regional dextral relative motion (indicated by arrows) is inferred [*Wheeler and Karson, 1994*].

man et al., 1995] dealt specifically with the subsidence of pull-apart basins as applied to the Dead Sea pull-apart basin. Here we generalize the study by comparing three cases: a single semi-infinite fault, several parallel faults, and overlapping en echelon faults. The effects of small oblique movements and faults with finite shear strength are also explored.

Deformation Along Strike-Slip Faults

Before we turn to the description of the various models and their results, we highlight several examples of ambiguities in the interpretation of deformation observed along strike-slip faults. Numerical models such as the ones presented in this paper can be used to eliminate some of the proposed interpretations in these regions and highlight plausible ones.

The kinematic interpretation of many continental rift systems (such as the Baikal and the East Africa) is being debated because the basin stratigraphy often indicates perpendicular extension, whereas the regional plate motion or motion on individual faults indicates a large component of strike slip [e.g., *Scott et al., 1989; Hutchinson et al., 1992*]. A well-studied ex-

ample is the Rukwa rift within the East African rift system (Figure 1). The rift is a 300-km-long half graben which is bounded on the NE side by the Lupa Fault [*Wheeler and Karson, 1994*]. The strata in the basin dip toward the Lupa Fault, except in the NW end of the basin, where they dip to the SE parallel to the fault. The depocenter is close to the SE tip of the fault. The SE tip of the fault ends in the Rungwe volcanic field, which is inferred to be a "strong zone" resistant to faulting [*Wheeler and Karson, 1994*]. Fault plane solutions indicate right-lateral strike-slip motion on the Lupa Fault, and slickensides are generally subparallel to the fault with a shallow plunge to the WNW. *Wheeler and Karson* [1994] concluded that right-lateral fault kinematics dominated the Lupa Fault throughout the rift evolution but noted that the stratigraphy of the basin indicates fault-normal extension. They resolved this ambiguity by appealing to *Ben-Avraham and Zoback's* [1992] explanation of local rotation of the "far-field" stress field near a weak fault.

Several strike-slip faults cross the San Francisco Bay region, some of which are parallel with the plate boundary and some

of which are slightly oblique. Many Plio-Quaternary compressional structures, folds, and reverse faults are parallel or oblique to the major strike-slip faults but are coeval. *Aydin and Page* [1984] interpreted the compressional features in several areas, such as the East Bay Hills, as resulting from the interaction between two strike-slip fault zones. *Jones et al.* [1994], on the other hand, interpreted the compressive features to indicate a slight contractional relative plate motion in addition to the strike slip. *Simpson et al.* [1994] compared the elevation of the San Francisco Bay region relative to the coastal ranges and suggested that the area is under slight extension in addition to strike slip.

Pull-apart basins which develop between en echelon strike-slip faults are also often accompanied by features interpreted to indicate fault-normal extension. Some pull-apart basins such as the Gulf of Aqaba and the Cariaco Basin [*Ben-Avraham*, 1992] are asymmetric. Normal faults are subparallel to strike-slip faults in the Dead Sea basin [*Ben-Avraham and Zoback*, 1992], and magmatic intrusions and volcanic eruptions occur along the strike-slip fault planes in the Erzincan and Nizic basins of western Turkey and in the western Basin and Range [*Aydin et al.*, 1990]. *Ben-Avraham and Zoback* [1992] suggested that extension perpendicular to the transform direction, caused by rotation of the principal stresses in a slightly divergent plate boundaries, is responsible for the development of some pull-apart basins. Another ambiguity is apparent in the study of pull-apart and push-up structures. The surficial dimensions of pull-apart basins and push-up ridges appear to obey a scale-invariant length-to-width ratio of 3:1 [*Aydin and Nur*, 1982], which contradicts earlier kinematic models that link the length of the feature to the amount of displacement on the fault [*Freund and Garfunkel*, 1976].

The models presented in this paper offer a different explanation for the development of "extensional" features in the vicinity of pure strike-slip fault systems. We also discuss the dependence of the length-to-width ratio of basins and push-up structures on the applied boundary conditions.

Model

Earthquakes at transform plate boundaries in most continental settings are predominantly confined to shallow depths (<15–20 km). Their confinement may be due to the change of deformation mechanism from pressure-sensitive brittle frictional sliding at shallow depths to temperature-sensitive aseismic ductile flow at larger depths [e.g., *Meissner and Strehlau*, 1982]. Alternatively, the confinement to shallow depths may be due to the transition in the frictional response of the fault from velocity weakening at shallow, cooler depths to velocity strengthening at greater depths [*Tse and Rice*, 1986]. With both explanations, stresses are substantially relaxed below the levels required for rapid slip, although postseismic slip is suggested to occur for a few years over a depth of 3–4 km below the seismogenic zone [*Tse and Rice*, 1986]. Using this rheological view of the crust, *Li and Rice* [1987] modeled crustal deformation due to earthquake cycles by coupled elastic upper crust and a viscoelastic lower crust, which are loaded from below by a steady "relative" plate-driving motion which increases (in opposite directions) away from the fault (Figure 2a). They found a good fit to geodetic strain rate across the San Andreas Fault with the lower crust having an effective viscosity of 2×10^{18} – 10^{19} Pa s and a relaxation time which is $\leq 10\%$ of the duration of the earthquake cycle. *King et al.* [1988] and *Stein et*

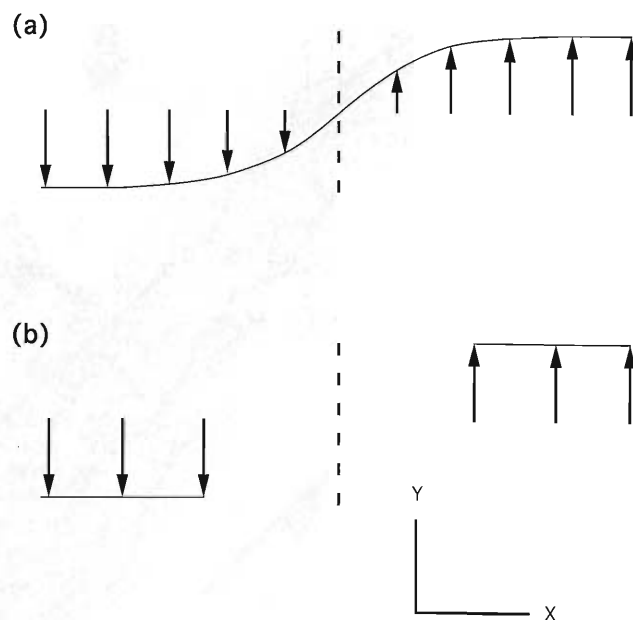


Figure 2. Illustration of two possible displacements imposed as boundary conditions at the base of the upper crust near strike-slip faults: (a) Displacement monotonously changes over a finite width area in the vicinity of the fault, resulting in the introduction of basal drag or drive [cf. *Li and Rice*, 1987]. (b) Upper crust is regionally displaced by plate relative motion, but an area in the vicinity of the fault (the "shear zone") has negligible basal drag or drive.

al. [1988] proposed that dip-slip geological structures result from the sum of processes occurring over many earthquake cycles, each of which can be regarded as having, on average, the same rheological and stress conditions and deformation field. Although their models involved an elastic plate overlying a viscoelastic half-space, they showed that successful modeling of surficial geological structures associated with normal and reverse faults did not require the full viscoelastic treatment. Stresses in the viscous substrate could, in effect, be regarded as completely relaxed over several earthquake cycles. Following this view, we study the long-term geological deformation at the surface with a single layer representing a 15-km-thick upper crust. The lower crust and the upper mantle are not modeled explicitly.

Because of its composition the upper mantle is generally the strongest part of the lithosphere and is therefore expected to carry the stresses due to plate motions [*Molnar*, 1992]. Because lithospheric plates move coherently, the upper crust is expected to ride passively together with the lower crust on the upper mantle, except near plate boundaries, where local interaction between the plates may exert large enough stresses to cause the upper crust to partially decouple and move independently from the upper mantle. Observations also suggest that some strike-slip faults in California may terminate at depth in midcrustal detachments [e.g., *Hearn and Clayton*, 1986; *Hudnut et al.*, 1988; *Nicholson et al.*, 1986, 1994] and may therefore be locally decoupled from the motion in the upper mantle. Our model assumes that upper crustal deformation is driven from below by the relative plate motion in the upper mantle. The driving motion is modeled by displacement that is specified on the bottom boundary of the model everywhere, except in a zone of finite width in the vicinity of the fault, which we call the

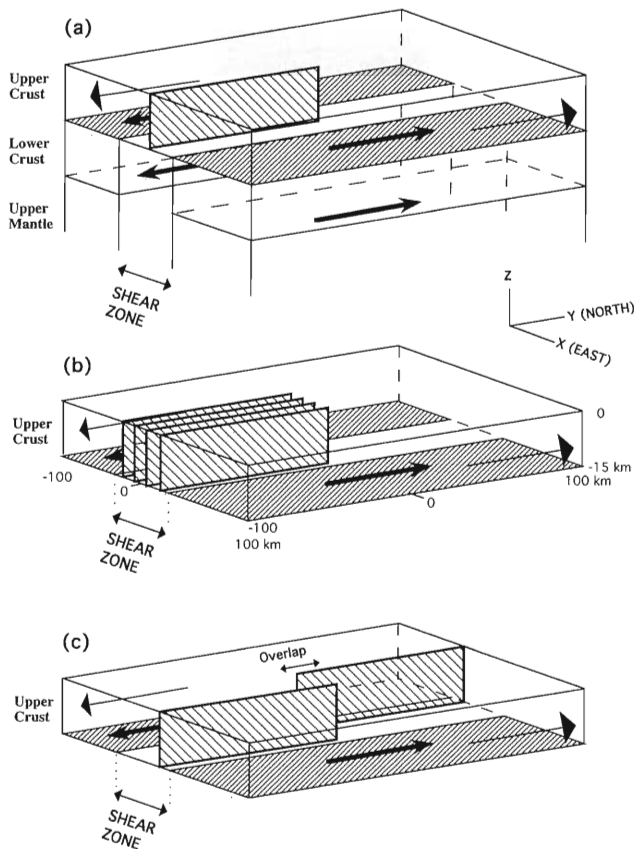


Figure 3. Block diagrams of the model geometries presented in this paper: (a) single vertical semi-infinite fault, (b) four parallel semi-infinite faults, and (c) overlapping en echelon faults. Arrows indicate displacement defined as a boundary condition. Displacement of equal amount and opposite direction is applied at the base and on the sidewalls of the model, but the base of the model in the vicinity of the fault(s) (the shear zone) is freely deforming. Figure 3a indicates that basal displacement of the upper crust is generated by a coherent movement of the entire lithosphere.

low-strength “shear zone” (Figures 2b and 3). Within this shear zone we assume that the upper crust is detached from the lower crust and can adjust itself by moving in all directions (including vertically). For completion, however, we also include a model with zero-width shear zone, namely, displacements are entirely predetermined at the base of the upper crust. Such a model can be considered to represent a narrow fault zone continuing into the lower crust. We also contrast the bottom-driven model with a model where displacement discontinuity is prescribed on the fault.

We use a 3-D boundary element commercial package, the Boundary-Element Analysis System (BEASY), developed by Computational Mechanics Inc., Billerica, Massachusetts. The model block is 200 km long (300 km for the case of en echelon faults), 200 km wide, and 15 km thick (Figure 3). The faults are oriented in the y direction and extend from the southern edge of the model (from both the southern and northern ends for the case of en echelon faults) to the middle of the block model and are 100 km long (160 km for en echelon faults). These dimensions ensure that edge effects are minimized in the center of the model where the effects of fault termination (pull-apart basins, subsidence and uplift, fault rotation) are investi-

gated. Faults are represented by vertical planes of weakness cutting through the entire depth of the plate on which no shear (tangential) stress is allowed. The assumption of weak strike-slip faults is supported by the observation of low-heat flow above the San Andreas Fault [Lachenbruch and Sass, 1992]. We also present, however, a set of models with faults having a finite strength and compare the resultant deformation with that from weak fault models.

A basal displacement of 2.5 km in the positive y direction (northward) is defined at $x > x_0$ (east of the fault zone), and a negative y displacement (southward) of 2.5 km is defined at $x < -x_0$ (west of the fault zone), where x_0 is the half width of the shear zone. Zero displacement in the x and z directions is defined at $x > |x_0|$. The same displacements are applied on the eastern and western walls of the model ($x = 100$ km, $x = -100$ km). These displacement boundary conditions create a left-lateral relative motion in the model. (The reader can apply the model results to right-lateral strike-slip fault systems by considering the results for right-lateral systems to be mirror images of the results presented here.) For the cases of oblique extension and contraction, displacement of 0.25 km is defined in the x direction away from or toward the fault zone. We do not define the displacements at the base of the shear zone ($-x_0 < x < x_0$) or at the surface, and these boundaries remain stress-free.

Our model is elastic. Laboratory measurements indicate, however, that upper crustal rheology is elastic plastic [e.g., Brace and Kohlstedt, 1980]; that is, stresses increase with strain up to a limit, beyond which failure occurs, and strain can increase significantly without comparable change in stresses. On a geological scale, stresses remain at a level typical to one earthquake cycle, whereas strain continues to accumulate during repeated earthquakes. We therefore define both the boundary conditions and the results in terms of displacement and refrain from including isostasy or body forces. Nevertheless, because the rheology is approximate, we use the elastic models to only investigate spatial patterns and relative amplitudes of deformations and not their absolute quantities. Because elastic rheology is linear, the amount of deformation in this study will be scaled by the amount of relative driving displacement.

We use a Poisson’s ratio of 0.5 (incompressible material) in order to conserve the rock volume over finite strains and geological timescales. Tests show that the resultant deformation pattern with a Poisson’s ratio of 0.5 is similar to that with a Poisson’s ratio of 0.25, but the magnitude of deformation is larger for the 0.5 case [Katzman *et al.*, 1995, Appendix B and Figure 15]. The Young’s modulus is set to 75 GPa. Because a linear elastic rheology is used, reduction of Young’s modulus by some factor will decrease the stresses by a similar factor but will not affect the stress pattern or the resulting displacement.

Results

We model the deformation around three simple fault geometries: a single fault extending from the edge to the center of a block (Figure 3a), four parallel faults extending from the edge to the center of a block (Figure 3b), and two overlapping faults extending from opposite edges to the center of block (Figure 3c).

A Single Fault

Models with a single-fault geometry allow us to examine deformation that is not influenced by fault interaction. The

deformation is caused by the need to accommodate the termination of the fault in an unfaulted zone and is dependent on the width of the shear zone, the shear strength of the fault, and the prescribed basal displacements.

Uplift and subsidence. Model results show an antisymmetric pattern of vertical motion with uplift on the east side of the fault tip and subsidence on the west side (Plate 1 and inset in Figure 4a). This pattern is caused by a decrease in displacement from the freely sliding region to the unfaulted region, resulting in material piling on the east side and stretching on the west side [Chinnery, 1961; Bilham and King, 1989]. In models where a constant displacement discontinuity is prescribed as a boundary condition on the fault, the patterns of uplift and subsidence are circular (Plate 1d) [Chinnery, 1961; Bilham and King, 1989]. In our models, which are driven by basal displacement, the predicted uplift and subsidence stretch along the fault, and a circular pattern no longer exists (Plates 1a–1c).

The width of the shear zone at the base of the upper crust has a considerable effect on the deformation near the fault tip: The magnitude of subsidence and uplift decreases with increasing width of the shear zone, but it is distributed over a larger area (Plate 1). The aerial increase of uplift and subsidence mainly occurs by distributing the deformation along the fault farther from the fault tip (Figure 4b) and to a lesser extent, by widening the deformed area (Figure 4a). As a result, the basins along strike-slip faults become more elongate with increasing width of the shear zone.

The dependence of the deformation pattern on the width of the shear zone for the basal-driven models is a consequence of the slip distribution along the fault. The deformed grid lines in Plates 1a–1c show a decrease in offset across the fault toward the fault tip. This decrease (or tapering) is a by-product of the basal-driven model. Slip on the fault tapers more slowly toward the tip when the shear zone is wide (Plate 1c) than when it is narrow (Plate 1a), causing the deformation to be spread along the fault and to be less concentrated near the tip. Slip distribution varies with the width of the shear zone only in models where the driving displacement is applied from below. In models where the driving displacement is applied on the sides of the models (i.e., across the entire thickness of the elastic layer) and where the fault plane is weak, the predicted deformation pattern does not change with the width of the shear zone [e.g., Katzman *et al.*, 1995, Figure 7c].

Effects of fault strength. The effect of the long-term strength of the fault is investigated by replacing the condition of zero shear strength on the fault with internal springs, which operate in the y (along the fault) and z (vertical) directions (Plate 2). The stiffness of the spring was scaled to the shear modulus [Crouch and Starfield, 1983, p. 208], which in many crustal rocks has the value of about 25 GPa [Turcotte and Schubert, 1982, p. 432]. We compare the deformation around faults having two levels of shear strength (2% and 10% of the shear modulus) to the deformation around a weak fault for models with 10-km basal shear zones (compare Plates 2a and 2b against 1b) and for models with 40-km basal shear zones (compare Plates 2c and 2d against 1c). Uplift and subsidence in the vicinity of strong faults decrease in amplitude with increasing fault strength. The pattern of uplift and subsidence becomes quasi-circular and concentrated near the fault tip, and slip distribution along the fault becomes almost constant, as can be observed from the offset of grid lines across the fault.

Another major difference between models with strong and weak faults is that strike-slip deformation is distributed in a

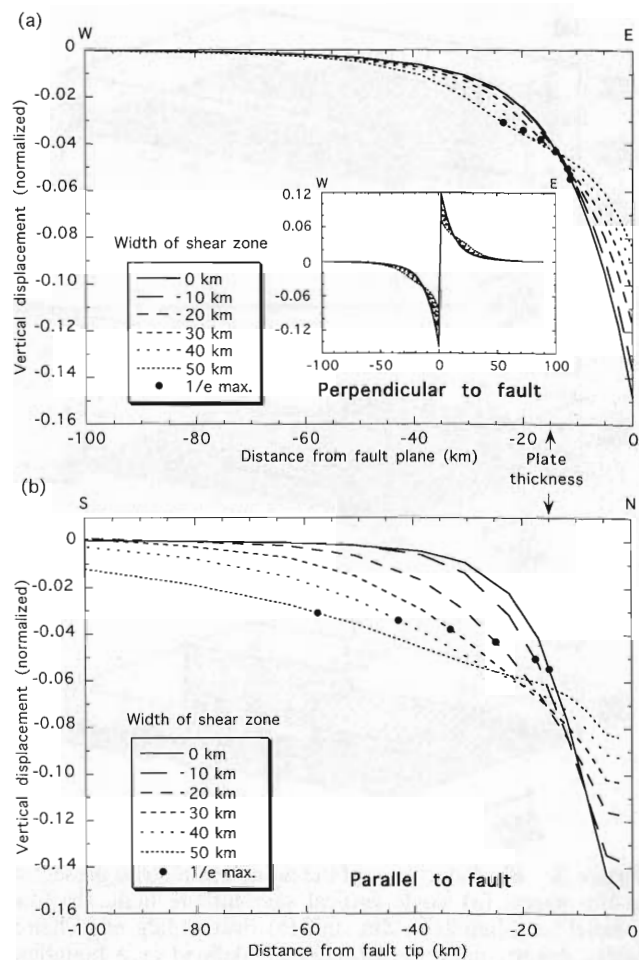


Figure 4. (a) Cross sections of vertical deformation (normalized to the amount of imposed displacement) perpendicular to and westward of the tip of a semi-infinite fault for models with different widths of the shear zone. (Inset) Same cross section with uplifted (eastward) side included. (b) Cross sections of vertical deformation parallel to and immediately westward of the fault trace for models with different widths of the shear zone. Dots indicate distances in which subsidence is $1/e$ of maximum subsidence for that model.

finite area around a strong fault, whereas the area surrounding a weak fault is relatively underformed (compare the grids in Plates 1 and 2). The deformed area around the fault becomes wider with increasing width of the shear zone (compare Plate 2a with 2c). With increasing fault strength, more deformation is distributed around the fault, and less deformation is taken as slip on the fault (compare Plate 2a with 2b). The magnitude of uplift and subsidence decreases with increasing fault strength, as the differential slip between the fault itself and the unfaulted crust decreases.

Horizontal displacements and fault plane rotations. Vertical displacements are only part of the deformation occurring near the ends of weak faults. Three-dimensional models allow the examination of displacements perpendicular to the fault plane. The amplitude of fault-normal displacements reaches as much as 50% of the vertical displacement near the fault's end for both the narrow (Plates 3a versus 1a) and wide (Plates 3b versus 1b) basal shear zone models. The fault-normal displacement decreases in amplitude with depth, resulting in a clock-

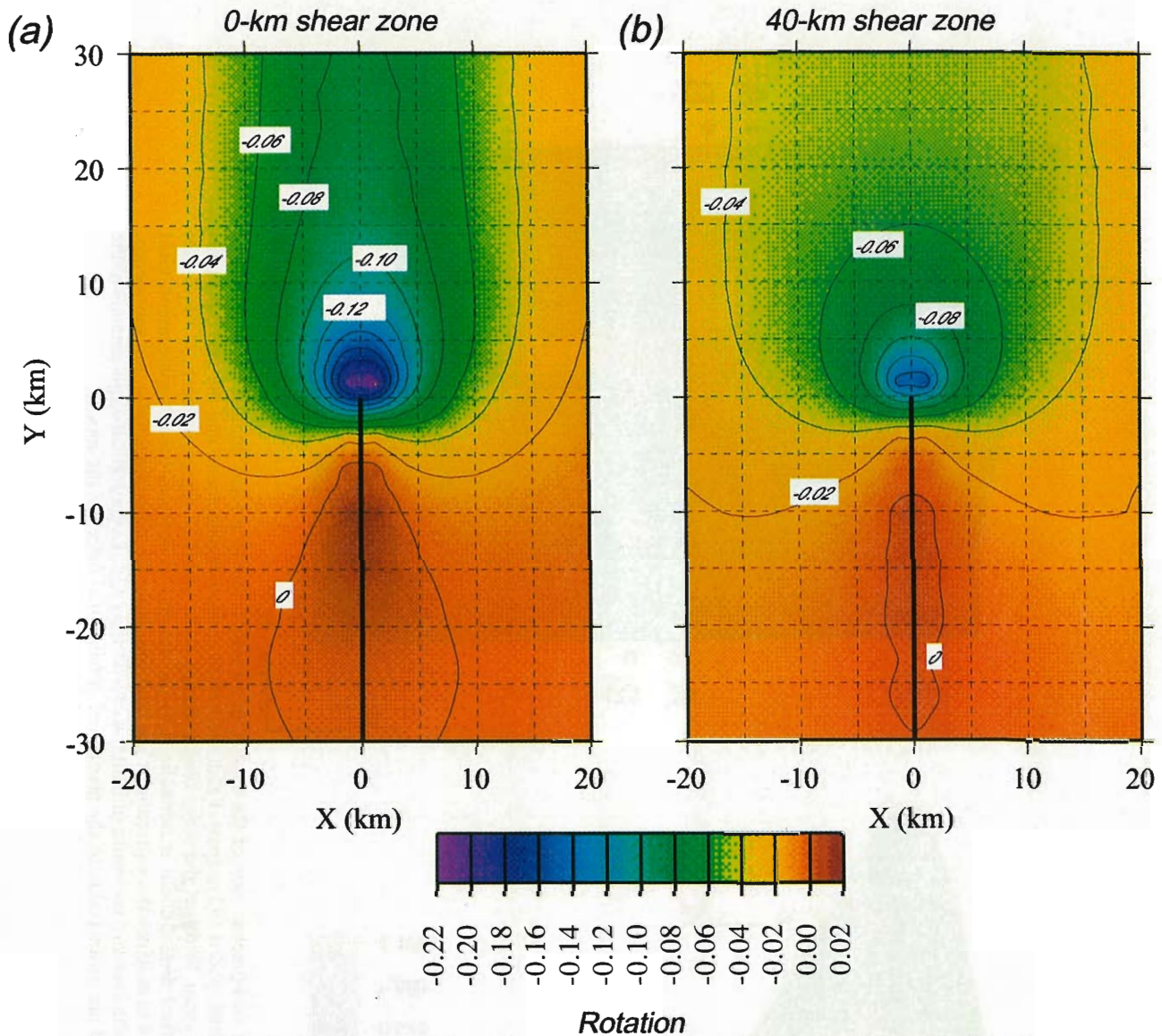


Plate 4. Rotation (in radians) around a vertical axis in the vicinity of a single semi-infinite fault tip due to left-lateral basal displacement with (a) 0-km-wide shear zone, and (b) 40-km-wide shear zone. Contour interval is 0.02 rad. Negative values represent counterclockwise rotation.

wise rotation of the fault plane around the horizontal y axis (Plate 3). (All directions pertain to left-lateral displacement and should be reversed in right-lateral systems). The clockwise rotation causes a small eastward turn (positive x direction) in the surface fault trace. Rotation diminishes as the width of the basal shear zone increases (Plate 3b). Curved fault traces are observed in seismic sections and sandbox models of strike-slip fault zones (Figure 5), although often they are interpreted to indicate a component of oblique slip [Harding, 1983]. Naylor *et al.* [1986] and Richard and Cobbold [1990] explained fault plane rotation as a consequence of rotation of the principal stresses from the bottom boundary where they are induced by the basal horizontal shear to the top where they must be orthogonal to the free surface.

In addition to vertical and horizontal displacements and fault plane rotation the models also suggest the development of counterclockwise surface rotation (in a left-lateral displacement) around the vertical axis ahead of the fault tip (Plate 4).

The magnitude of the rotation increases with decreasing width of the basal shear zone. This relationship is due to the fact that slip on the faults tapers more rapidly toward the tip when the shear zone is narrower. The rotation, together with the uplift and subsidence, accommodate the change from the fault to the unfaulted zone.

Parallel Faults

Strike-slip deformation along plate boundaries is often distributed among several parallel faults such as in the North American-Pacific plate boundary in northern and southern California [Page, 1990]. We examine the surface deformation around parallel faults using a model with four parallel planes of zero shear strength on which the displacement is distributed (Figure 3b). The faults extend from the southern boundary to the center of the block model, and they are 10 km apart at $x = -15, -5, 5,$ and 15 km. The width of the shear zone at the bottom is 60 km (four plate thicknesses) or 15 km on either

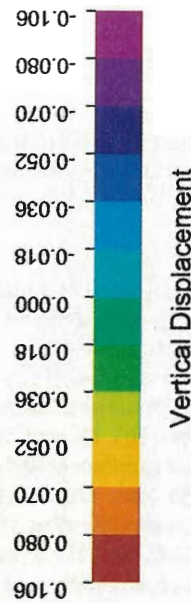
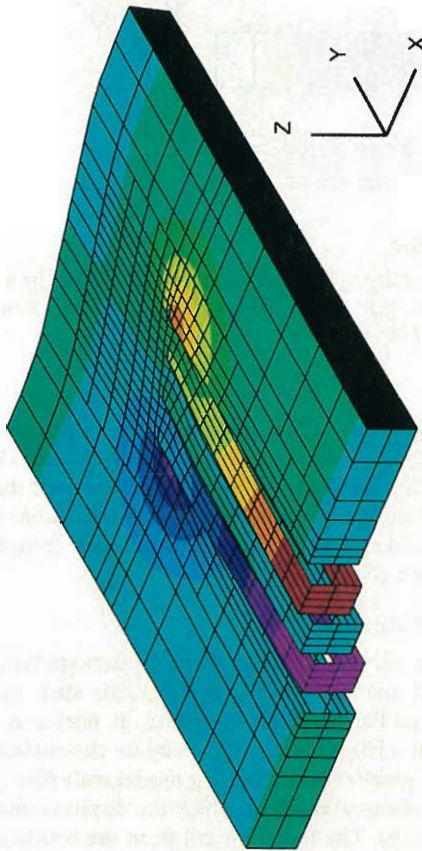
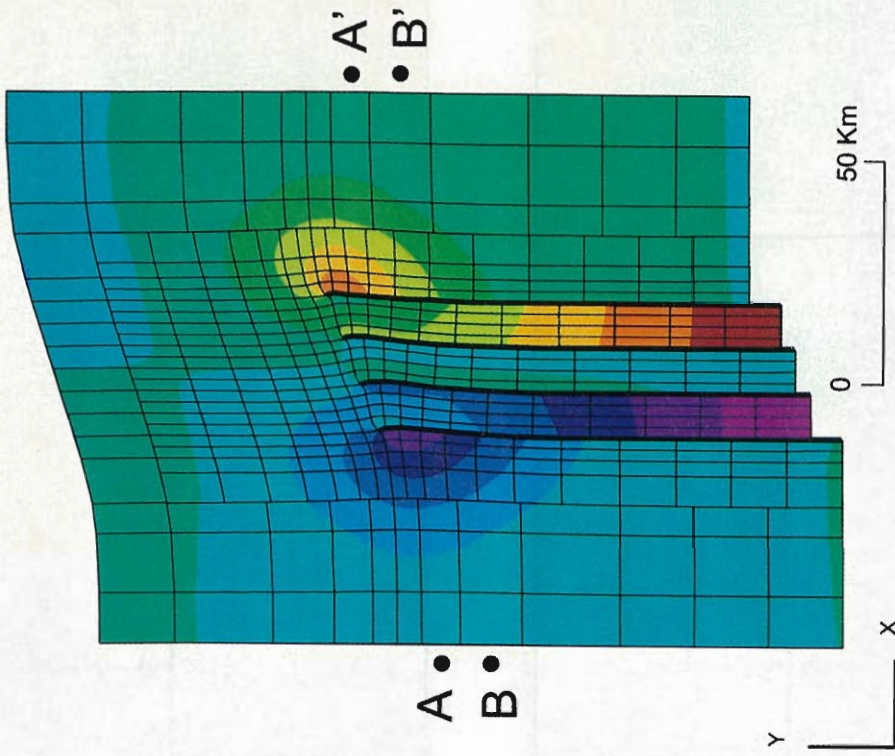


Plate 5. (right) A plan view and (left) an isometric view of the surface deformation due to a 5-km relative left-lateral basal motion and four parallel semi-infinite faults spaced 10 km apart. Colors represent vertical displacement, and the grid represents deformation from originally rectangular mesh. Width of the shear zone is 60 km. A-A' and B-B' represent locations of profiles in Figures 6a and 6b, respectively. Vertical displacement is normalized to the amount of imposed basal displacement. Grid deformation is multiplied by a factor of 4 to enhance the pattern near the fault tips. Note the differential uplift and subsidence, the tilt of the fault-bounded blocks, and the eastward curvature of fault traces near their tips. Large vertical displacements of the blocks in the southern end of the model are artifacts due to the absence of gravitational forces in the model.

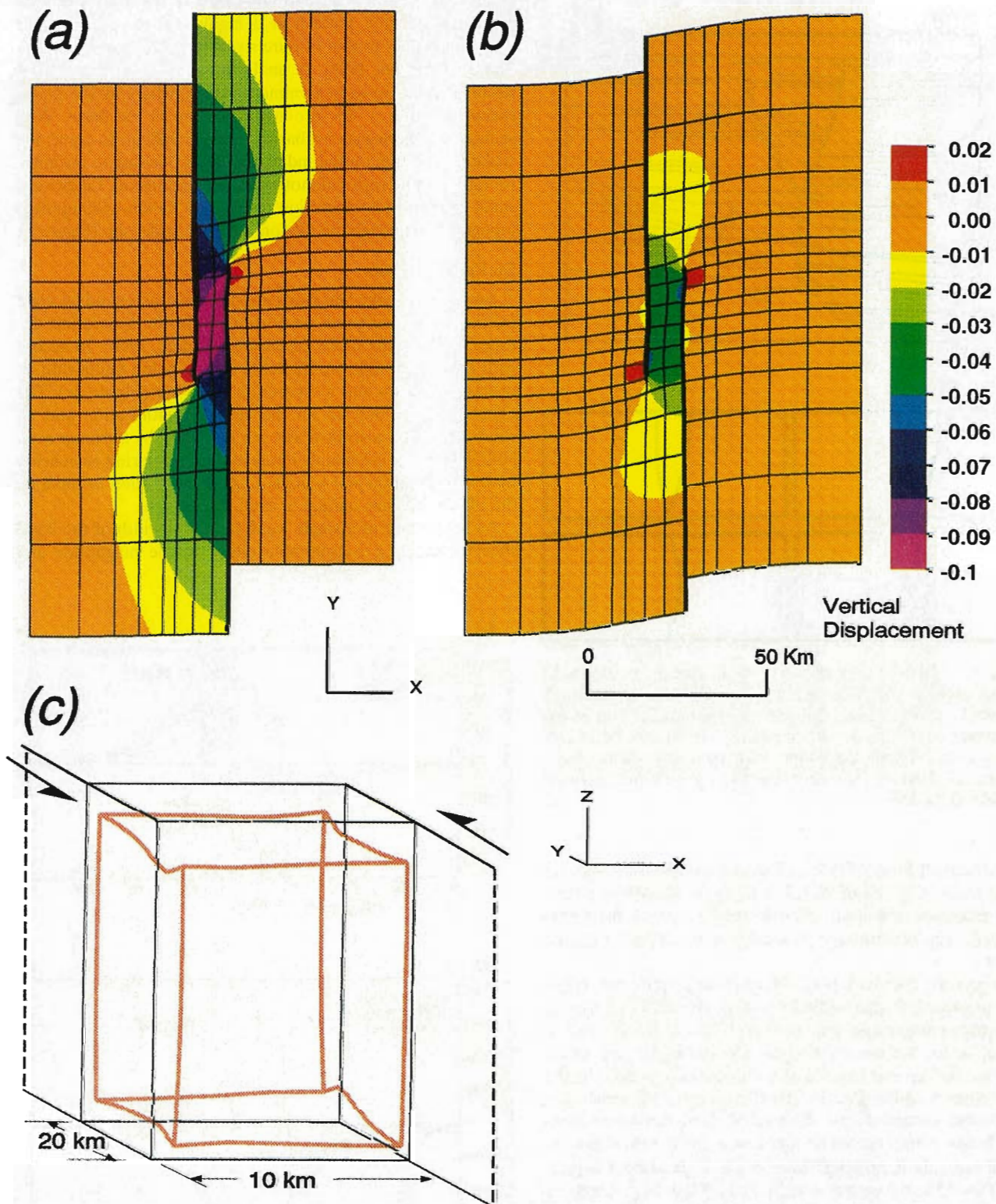


Plate 6. Surface deformation due to an imposed 5-km relative left-lateral basal motion in a model with (a) weak (zero shear strength) and (b) strong (2% of the shear modulus of the medium) en echelon semi-infinite faults. The faults are spaced 10 km apart and overlap by 20 km (see Figure 3c). Colors represent vertical displacement (normalized to the amount of imposed basal displacement), and the grid represents deformation from originally rectangular mesh. Width of the shear zone is 40 km. (c) Isometric view of the volume enclosed by the overlapping faults before deformation (indicated by black lines) and after deformation (indicated by red lines) in the weak fault model. Note that the volume in Plate 6c deforms almost in pure shear, extending in the y direction and contracting in the z and x directions. Deformed grids in Plates 6a and 6b are multiplied by a factor of 4 to enhance the pattern.

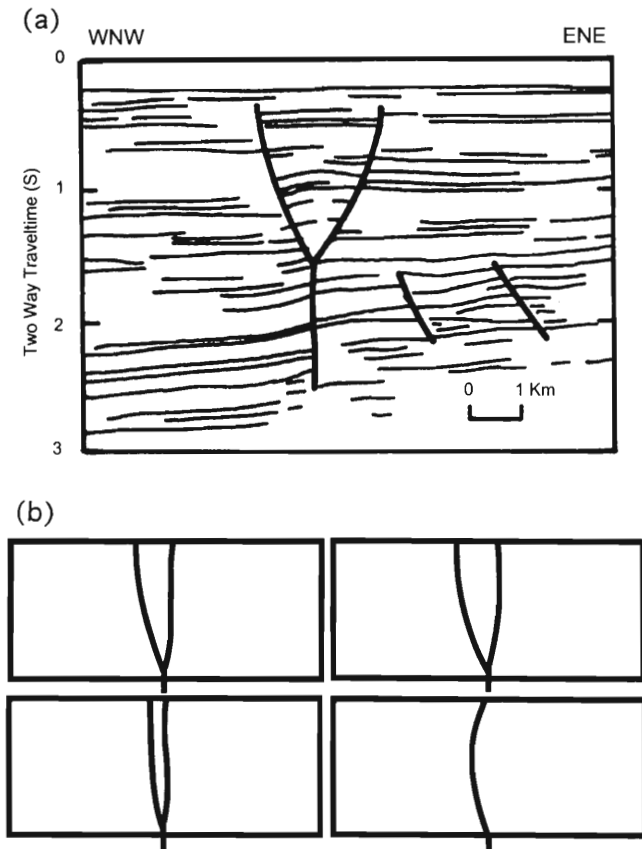


Figure 5. (a) Line drawing of seismic section in Scotland showing convex upward fault pattern (modified from *Naylor et al.* [1986]). (b) Four cross sections through wrench fault zones in sandbox experiments with imposed basal pure strike slip [*Naylor et al.*, 1986]. Reprinted with kind permission from Elsevier Science Ltd, The Boulevard, Langford Lane, Kidlington OX5 1GB, UK.

side of the fault zone. All other dimensions and parameters are similar to the single-fault model. The results show that a variety of extension and contraction features can arise from parallel strike-slip deformation with little or no oblique regional motion.

The general distribution of antisymmetric uplift and subsidence produced by parallel faults' models (Plate 5) is similar to the pattern produced by a single fault (Plate 1). In the case of parallel faults, however, the antisymmetric uplift and subsidence are broken into a series of tilted blocks separated by the faults (Plate 5 and Figure 6). The fault planes themselves are also rotated clockwise near the surface from vertical to high-angle faults, giving the appearance of a small component of normal separation, although the driving displacement is pure strike slip. As in the case of a single fault (Plate 3), the surface traces of parallel faults curve slightly eastward toward the fault tips. Vertical and horizontal displacement perpendicular to the fault plane, fault plane rotation, and curvature of the fault trace all have a larger magnitude than in the case of a single fault because the continuum is now broken in several locations and cannot sustain shear stresses there.

When the entire strike-slip fault system is subjected to a small amount of oblique opening or closing (5° or 10% of the relative sinistral motion), the entire deformed fault zone either subsides or uplifts, but the internal deformation is unchanged

(Figure 6). Clay models and numerical simulations also indicate that the fault pattern at a highly oblique rifting angle ($<30^\circ$) is similar to that of pure strike slip [*Withjack and Jamison*, 1986; *Braun*, 1994]. A small amount of oblique opening results in a 60-km-wide asymmetric basin, where all the faults, except that at $x = 15$, are at the bottom of the basin. With sediments covering such a basin it may be difficult to detect the strike-slip motion on the individual faults, leading to misinterpretation of the regional motion as pure extension. Likewise, a small amount of compression results in a 60-km-wide uplifted topography, although the motion is mainly strike slip (Figure 6).

En Echelon Faults

En echelon strike-slip faults are often characterized by slight overlap which increases proportionally to the separation distance between the faults [*Aydin and Schultz*, 1990]. In accord with this observation we model two en echelon faults with an overlap of 20 km and a separation of 10 km (Figure 3c). The effects of fault overlap on the vertical deformation and on rotation around a vertical axis are discussed by *Katzman et al.* [1995]. Here we are mainly interested in comparing en echelon fault configuration and a single-fault configuration to separate the effects that are unique to fault interaction.

As in the case of a single weak fault, the width of the basal shear zone has a considerable effect on the magnitude and

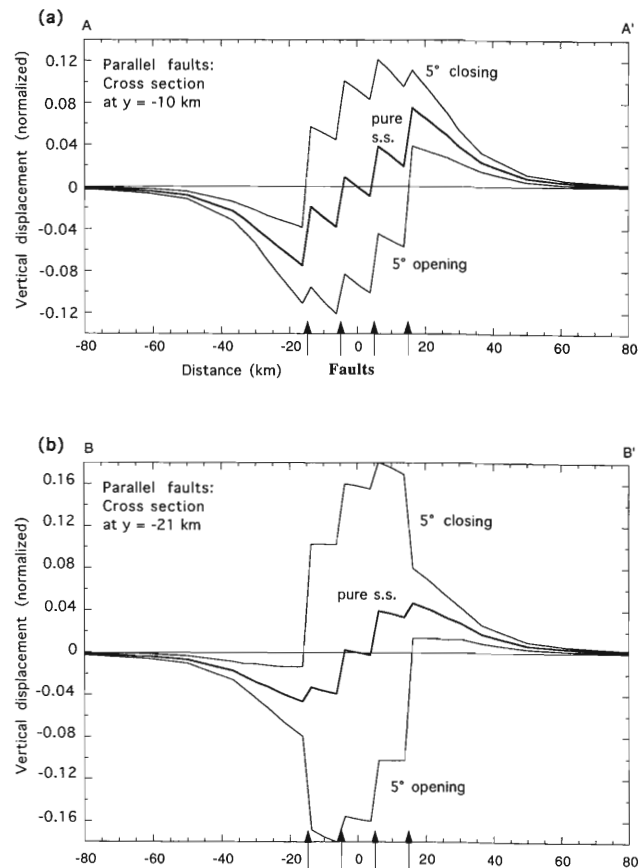


Figure 6. Vertical deformation (normalized to the amount of imposed basal displacement) due to pure strike slip (indicated by heavy lines) and oblique motion of 5° (indicated by thin lines) along cross sections perpendicular to the four parallel semi-infinite faults at (a) 10 km and (b) 21 km south of the fault tips (see Plate 5 for locations).

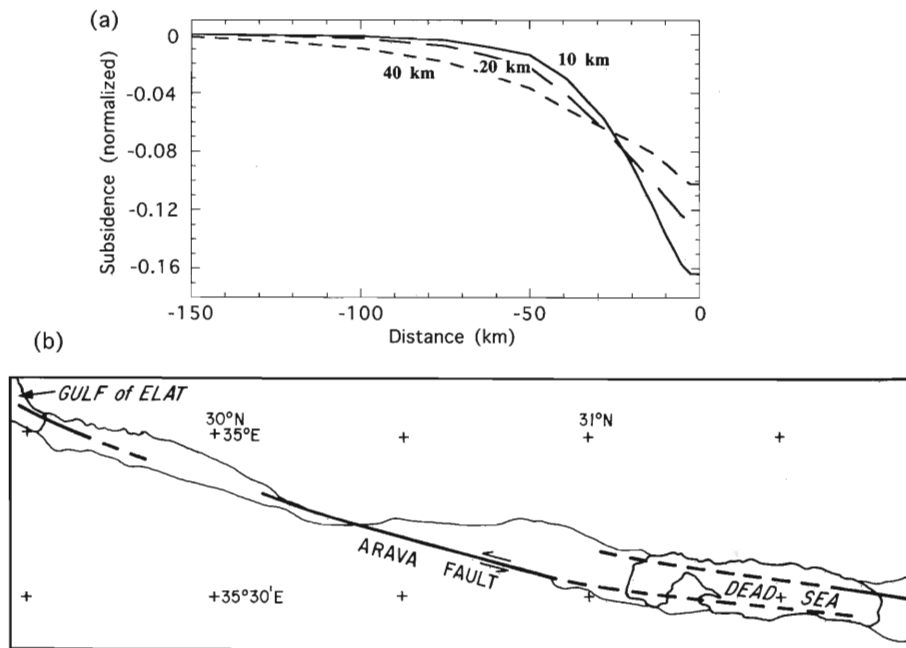


Figure 7. (a) Subsidence (normalized to the imposed left-lateral displacement) along the axis of a pull-apart basin as a function of the width of the basal shear zone in a model with two en echelon semi-infinite faults spaced 10 km apart and terminating without an overlap [Katzman *et al.*, 1995]. Note that the basin lengthens with increasing width of the shear zone (similar to Plate 1b). (b) An example from the Dead Sea transform where the subsidence (areas enclosed by thin lines) extends up to 100 km from the Dead Sea pull-apart basin and from the Gulf of Elat (Aqaba) [Garfunkel, 1981].

length of subsidence (pull-apart basins) or uplift (push-up structures) between the faults (Figure 7a) [Katzman *et al.*, 1995]. The subsidence (or uplift) is shallower and longer for a wider shear zone. The distribution of the deformation is determined by the rate of decrease of slip toward the ends of the faults. Because the tapering of slip is gradual, pull-apart basins are expected to shallow gradually away from the overlapping area. This result is supported by geological observations. For example, the Dead Sea transform valley is occupied by the extensions of pull-apart basins developed along en echelon faults far beyond the overlapping areas (Figure 7b) [Garfunkel, 1981]. Geophysical data indicate that the depth of the Dead Sea pull-apart basin decreases gradually from the center of the basin to its southern end [ten Brink *et al.*, 1993]. The model suggests that a 20- to 40-km-wide shear zone at the base of the crust may create these elongate basins within the Dead Sea transform.

The uplift near the tips of en echelon faults is small relative to the subsidence of the basin bounded by the overlapping fault strands (Plate 6a and Figure 8), unlike the case of a single fault, where uplift and subsidence have almost similar magnitudes (Plate 1). This is because the slip between the two crustal blocks does not end at the tip of the fault but continues along the second fault. Therefore the two blocks are effectively slipping along their entire boundary, even in the absence of cross faults connecting the en echelon faults, and crustal material sliding along the faults is hardly compressed against a locked zone at the end of the faults.

When en echelon faults have a finite shear strength, the amount of subsidence of pull-apart basins and their total length diminish considerably (Plate 6b). Part of the deformation is distributed in a wide zone outside the fault system. The amount of uplift near the faults' ends, on the other hand,

remains the same as in the case of weak faults. Hence, for strong faults the amplitudes of subsidence and uplift are of similar size and both are small.

Additional model runs (not shown here) verify that left-stepping en echelon faults subjected to right-lateral basal motion produce an uplift (push-up structures) with a distribution which is identical to the distribution of subsidence in Plate 6. The absolute magnitudes of subsidence and uplift are also the same because isostasy and body forces were not included in the model.

Another feature resulting from the interaction between the faults is the almost symmetrical subsidence (full graben) across the basin bounded by the overlapping faults (Figure 8a) [Katzman *et al.*, 1995]. The subsidence of the Dead Sea basin [ten Brink and Ben-Avraham, 1989; ten Brink *et al.*, 1993] and the Erzincan basin [Hempton and Dunne, 1984] are, indeed, fairly symmetric between the overlapping strands and appear to have their deepest part located between the overlapping segments of the faults. Outside the overlap zone, subsidence is antisymmetric (half graben) as in the case of a single fault. Fault interaction is also responsible for fault-normal extension. Our 3-D model shows that the block enclosed between overlapping weak faults is deformed almost in pure shear by lengthening along the y axis and by contracting in both the vertical (subsidence) and the fault-perpendicular (x direction) axes (Plate 6c). Using a 2-D boundary element model, Aydin *et al.* [1990] produced fault-normal extension in the region of overlapping strike-slip faults. There is therefore no need to invoke divergent plate motion [Ben-Avraham and Zoback, 1992] to explain extensional features along strike-slip faults.

Small amounts of oblique opening and closing (5°, or about 10% of the strike-slip motion) do not change the cross-sectional geometry of the pull-apart basin but add a large

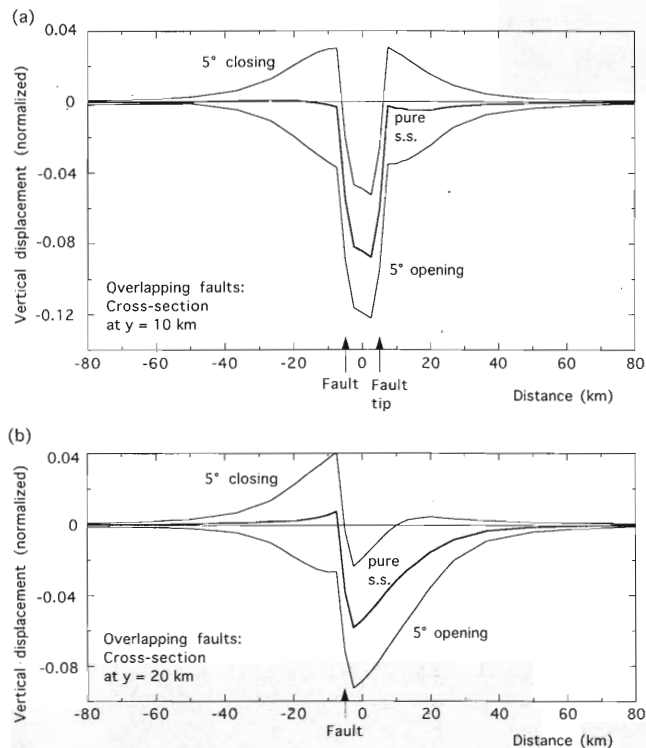


Figure 8. Cross sections of the surface vertical deformation perpendicular to the en echelon faults in Figure 7a: (a) at 10 km from the center of the overlapping area, where the profile crosses both faults, and (b) at 20 km from the center of the overlapping area, where the profile crosses only one fault. Heavy lines indicate deformation due to pure strike slip. Thin lines indicate deformation due to imposed basal oblique extension or compression at a 5° angle to the y axis (motion in the x direction is 10% of that imposed in the y direction). Vertical deformation is normalized to the imposed left-lateral displacement.

regional component of subsidence or uplift (Figure 8). Clay models and analytical models of oblique rifting with 15° opening indeed show that the style of deformation is similar to that of pure strike slip [Witjack and Jamison, 1986]. The oblique motion in the models thus makes the surface expression of sediment- or water-filled basins appear wider. As in the case of parallel faults, it may be difficult to identify the sense of motion on the buried faults, leading to an erroneous interpretation of the regional displacement field.

Discussion and Conclusions

The modeling results described in this paper underscore the difficulty in deducing the relative motion of plate or block boundaries from the local crustal deformation field. Several of the features produced by the model, such as elongate half grabens along a single fault, rotated blocks at the ends of parallel faults, or the extension perpendicular to overlapping en echelon strike-slip faults would be typically interpreted to indicate regional extension perpendicular to the fault. In addition, wide zones of uplift or subsidence are generated in models with several parallel faults which are subject to regional strike-slip displacement with only a minor oblique component of extension or shortening. These wide deformation zones

would ordinarily be interpreted to result primarily from regional extension or shortening and not from strike-slip motion.

The possible decoupling of the upper and lower crust in the vicinity of some strike-slip faults (wide shear zones) as opposed to the downward continuation of strike-slip faults in narrow zones in the lower crust (narrow shear zones) has a considerable impact on the surface deformation. We found that the width of the shear zone affects the rate of tapering of relative displacement toward the fault tips. The rate of tapering, in turn, controls the aerial extent and amplitude of the vertical and horizontal surface deformation such as the length of half grabens and pull-apart basins and the amounts of rotation around horizontal and vertical axes. For example, fault plane rotation is predicted to be particularly large for zero-width shear zones because basal movement adjacent to the fault is constrained, and therefore deformation can only spread upward and outward. A zero-width shear zone may be representative of strike-slip faults continuing downward into the lower crust in a narrow zone and is also typical of faults continuing upward from a coherent basement to less consolidated sediments.

Comparison between our models and field examples, reviewed earlier in the paper, indicates that models with weak faults fit the observations better than strong fault models. Models with weak faults generate elongate basins along the faults, whereas models with strong faults have more localized deformation at the tip of the faults. In particular, asymmetric basins along single faults, such as the Rukwa basin in East Africa (Figure 1), can be explained by pure strike-slip motion on a weak Lupa Fault. Models of weak overlapping en echelon faults generate large subsidence in the area of fault overlap and relatively very little uplift near the fault tips, whereas models with strong faults generate small but comparable amounts of subsidence and uplift. There is indeed little evidence for uplift near the fault tips in the Dead Sea [ten Brink et al., 1993], Erzincan [Hempton and Dunne, 1984], and Cariaco [Schubert, 1982] basins where subsidence is large. Finally, a pull-apart basin between two weak faults can reach tens of kilometers beyond the overlapping area (Figure 7a), in accord with observations along the Dead Sea rift (Figure 7b). Models in which the faults have no strength appear therefore to be a good approximation to long-term upper crustal behavior.

Our models indicate that for a given separation between faults the length of pull-apart basins increases with increasing width of the shear zone (Figure 7a). This contradicts Aydin and Nur's [1982] suggestion that the length-to-width ratio of pull-apart basins is 3:1. Their suggestion was made on the basis of measurements of the surface dimensions of basins; however, later geophysical data show that the dimensions of some basins (e.g., the Cholame valley [Shedlock et al., 1990] and the Dead Sea basin [ten Brink et al., 1993]) differ from their surface expression. Although the amount of overlap generally increases with the amount of separation between overlapping faults [Aydin and Schultz, 1990], which implies that longer basins are also wider, both the data and the model show that pull-apart basins may extend to different lengths beyond the zone of overlap (e.g., the Dead Sea basin [ten Brink et al., 1993]) (Figure 8b). Hence the length-to-width ratio of pull-apart basins is not expected to be constant.

Acknowledgments. Support for this study was provided by the U.S. Geological Survey marine program (to U.T.B. and R.K.) and by NSF

grant OCE-9300708 (to J.L.). We are grateful to Geoff King, Peter Molnar, Zeev Reches, and Ross Stein for fruitful discussions and to Ross Stein, Yang Shen, Richard Schultz, and an anonymous reviewer and an associate editor for constructive reviews of the manuscript. We thank J. Trevelyan from Computational Mechanics, Billerica, Massachusetts, for answering numerous questions regarding the BEASY boundary element code and A. Johnson for help with the figures. Contribution 8958 of the Woods Hole Oceanographic Institution.

References

- Aydin, A., and A. Nur, Evolution of pull-apart basins and their scale independence, *Tectonics*, *1*, 91–105, 1982.
- Aydin, A., and B. Page, Diverse Pliocene-Quaternary tectonics in a transform environment, San Francisco Bay region, California, *Geol. Soc. Am. Bull.*, *95*, 1303–1317, 1984.
- Aydin, A., and R. A. Schultz, Effect of mechanical interaction on the development of strike-slip faults with echelon patterns, *J. Struct. Geol.*, *12*, 123–129, 1990.
- Aydin, A., R. A. Schultz, and D. Campagna, Fault-normal dilatation in pull-apart basins: Implications for the relationship between strike-slip faults and volcanic activity, *Ann. Tecton.*, *4*, 45–52, 1990.
- Ben-Avraham, Z., Development of asymmetric basins along continental transform faults, *Tectonophysics*, *215*, 209–220, 1992.
- Ben-Avraham, Z., and M. D. Zoback, Transform-normal extension and asymmetric basins: An alternative to pull-apart models, *Geology*, *20*, 423–426, 1992.
- Bilham, R., and G. King, The morphology of strike-slip faults: Examples from the San Andreas fault, California, *J. Geophys. Res.*, *94*, 10,204–10,216, 1989.
- Brace, W. F., and D. L. Kohlstedt, Limits on lithospheric stress imposed by laboratory experiments, *J. Geophys. Res.*, *85*, 6248–6252, 1980.
- Braun, J., Three-dimensional numerical simulations of crustal-scale wrenching using a non-linear failure criterion, *J. Struct. Geol.*, *16*, 1173–1186, 1994.
- Chinnery, M. A., The deformation of the ground around surface faults, *Bull. Seismol. Soc. Am.*, *51*, 355–372, 1961.
- Christie-Blick, N., and K. T. Biddle, Deformation and basin formation along strike-slip faults, in *Strike-Slip Deformation, Basin Formation, and Sedimentation*, edited by K. T. Biddle and N. Christie-Blick, pp. 1–34, Soc. of Econ. Paleontol. and Mineral., Tulsa, Okla., 1985.
- Crouch, S. L., and A. M. Starfield, *Boundary Element Methods in Solid Mechanics*, 332 pp., Allen and Unwin, Winchester, Mass., 1983.
- Freund, R., and Z. Garfunkel, *Guidebook to the Dead Sea Rift*, 27 pp., Hebrew Univ., Jerusalem, 1976.
- Garfunkel, Z., Internal structure of the Dead Sea leaky transform (rift) in relation to plate kinematics, *Tectonophysics*, *80*, 81–108, 1981.
- Gomberg, J., and M. Ellis, Topography and tectonics of the central New Madrid seismic zone: Results of numerical experiments using a three-dimensional boundary element program, *J. Geophys. Res.*, *99*, 20,299–20,310, 1994.
- Harding, T. P., Divergent wrench faults and negative flower structures, Andaman Sea, in *Seismic Expression of Structural Styles*, vol. 3, *Tectonics of Compressional Provinces/Strike-Slip Tectonics*, Stud. Geol., vol. 15, edited by A. W. Bally, pp. 4.2-1 to 4.2-8, Am. Assoc. Pet. Geol., Tulsa, Okla., 1983.
- Hearn, T. M., and R. W. Clayton, Lateral velocity variations in southern California, II, Results from the lower crust from Pn waves, *Bull. Seismol. Soc. Am.*, *76*, 511–520, 1986.
- Hempton, M. R., and L. A. Dunne, Sedimentation in pull-apart basins: Active examples in eastern Turkey, *J. Geol.*, *92*, 513–530, 1984.
- Hudnut, K., L. Seeber, J. Pachelo, J. Armbruster, L. Sykes, G. Bond, and M. Kominz, Cross faults and block rotation in southern California: Earthquake triggering and strain distribution, *Lamont Res. Annu.*, 44–49, 1988.
- Hutchinson, D. R., A. J. Golmshtok, L. P. Zonenshain, T. C. Moore, C. A. Scholz, and K. D. Klitgord, Depositional and tectonic framework of the basins of Lake Baikal from multichannel seismic data, *Geology*, *20*, 589–592, 1992.
- Jones, D. L., R. Graymer, C. Wang, T. V. McEvilly, and A. Lomax, Neogene transverse evolution of the California Coast Ranges, *Tectonics*, *13*, 561–574, 1994.
- Katzman, R., U. S. ten Brink, and J. Lin, Three-dimensional modeling of pull-apart basins: Implications for the tectonics of the Dead Sea basin, *J. Geophys. Res.*, *100*, 6295–6312, 1995.
- King, G. C. P., R. S. Stein, and J. B. Rundle, The growth of geological structures by repeated earthquakes, 1, Conceptual framework, *J. Geophys. Res.*, *93*, 13,307–13,318, 1988.
- King, G. C. P., R. S. Stein, and J. Lin, Static stress changes and the triggering of earthquakes, *Bull. Seismol. Soc. Am.*, *84*, 935–953, 1994.
- Lachenbruch, A. H., and J. H. Sass, Heat flow from Cajon Pass, fault strength, and tectonic implications, *J. Geophys. Res.*, *97*, 4995–5015, 1992.
- Li, V. C., and J. R. Rice, Crustal deformation in great California earthquake cycles, *J. Geophys. Res.*, *92*, 11,533–11,551, 1987.
- Meissner, R., and J. Strehlau, Limits of stresses in continental crusts and their relation to the depth-frequency distribution of shallow earthquakes, *Tectonics*, *1*, 73–89, 1982.
- Molnar, P., Brace-Goetze strength profiles, the partitioning of strike-slip and thrust faulting at zones of oblique convergence, and the stress-heat flow paradox of the San Andreas fault, in *Fault Mechanics and Transport Properties of Rocks*, edited by T. F. Wong and B. Evans, Academic, San Diego, Calif., 1992.
- Naylor, M. A., G. Mandl, and C. H. K. Sijpesteijn, Fault geometries in basement-induced wrench faulting under different initial stress states, *J. Struct. Geol.*, *8*, 737–752, 1986.
- Nicholson, C., L. Seeber, P. Williams, and L. R. Sykes, Seismic evidence for conjugate slip and block rotation within the San Andreas fault system, southern California, *Tectonics*, *5*, 629–648, 1986.
- Nicholson, C., C. C. Sorlien, T. Atwater, J. C. Crowell, and B. Luyendyk, Microplate capture, rotation of the western Transverse Ranges, and initiation of the San Andreas transform as a low-angle fault system, *Geology*, *22*, 491–495, 1994.
- Page, B. M., Evolution and complexities of the transform system in California, USA, *Ann. Tecton.*, *4*, 53–69, 1990.
- Richard, P., and P. Cobbold, Experimental insights into partitioning of fault motions in convergent wrench zones, *Ann. Tecton.*, *4*, 35–44, 1990.
- Schubert, C., Origin of Cariaco basin, Southern Caribbean Sea, *Mar. Geol.*, *47*, 345–360, 1982.
- Scott, D. L., B. R. Rosendahl, C. F. Burgess, and S. Sander, Comment on “Variable extension in Lake Tanganyika” by C. K. Morley, *Tectonics*, *8*, 647–650, 1989.
- Segall, P., and D. D. Pollard, Mechanics of discontinuous faults, *J. Geophys. Res.*, *85*, 4337–4350, 1980.
- Shedlock, K. M., T. M. Brocher, and S. T. Harding, Shallow structure and deformation along the San Andreas Fault in Cholame Valley, California, based on high-resolution reflection profiling, *J. Geophys. Res.*, *95*, 5003–5020, 1990.
- Simpson, R. W., K. R. Lajoie, and D. H. Oppenheimer, Inferring blind thrusts in the San Francisco Bay region from earthquake focal mechanisms and averaged topography, *Eos. Trans. AGU*, *75*(44), Fall Meet. Suppl., 681, 1994.
- Stein, R. S., G. C. P. King, and J. B. Rundle, The growth of geological structures by repeated earthquakes, 2, Field examples of continental dip-slip faults, *J. Geophys. Res.*, *93*, 13,319–13,331, 1988.
- Stein, R. S., G. C. P. King, and J. Lin, Change in failure stress on the southern San Andreas fault system caused by the 1992 magnitude = 7.4 Landers earthquake, *Science*, *258*, 1328–1332, 1992.
- Sylvester, A. G., Strike-slip faults, *Geol. Soc. Am. Bull.*, *100*, 1666–1703, 1988.
- ten Brink, U. S., and Z. Ben-Avraham, The anatomy of a pull-apart basin: Seismic reflection observations of the Dead Sea basin, *Tectonics*, *8*, 333–350, 1989.
- ten Brink, U. S., Z. Ben-Avraham, R. E. Bell, M. Hassouneh, D. F. Coleman, G. Andeasen, G. Tibor, and B. Coakley, Structure of the Dead Sea pull-apart basin from gravity analysis, *J. Geophys. Res.*, *98*, 21,887–21,894, 1993.
- Tse, S. T., and J. R. Rice, Crustal earthquake instability in relation to the depth variation of frictional slip properties, *J. Geophys. Res.*, *91*, 9452–9472, 1986.
- Turcotte, D. L., and G. Schubert, *Geodynamics*, 450 pp., John Wiley, New York, 1982.
- Wheeler, W. H., and J. A. Karson, Extension and subsidence adjacent to a “weak” continental transform: An example from the Rukwa rift, East Africa, *Geology*, *22*, 625–628, 1994.
- Wilcox, R. E., T. P. Harding, and D. R. Seely, Basic wrench tectonics, *Am. Assoc. Pet. Geol. Bull.*, *57*, 74–96, 1973.
- Withjack, M. O., and W. R. Jamison, Deformation produced by oblique rifting, *Tectonophysics*, *126*, 99–124, 1986.

R. Katzman, Department of Earth, Atmospheric, and Planetary Sciences, Massachusetts Institute of Technology, Room 54-522, Cambridge, MA 02139. (e-mail: rafk@quake.mit.edu)

J. Lin, Department of Geology and Geophysics, Woods Hole Oceanographic Institution, Woods Hole, MA 02543. (e-mail: jlin@aqu.who.edu)

U. S. ten Brink, U.S. Geological Survey, Quissett Campus, Atlantic

Marine Geology, Woods Hole, MA 02543-1598. (e-mail: tenbrink@nobska.er.usgs.gov)

(Received March 24, 1995; revised January 19, 1996; accepted March 15, 1996.)